Topology and current ribbons: A model for current, reconnection and flaring in a complex, evolving corona

D.W. Longcope
Space Sciences Laboratory, University of California, Berkeley, CA 94720

ABSTRACT

Magnetic field enters the corona from the interior of the Sun through isolated magnetic features on the solar surface. These features correspond to the tops of submerged magnetic flux tubes, and coronal field lines often connect one flux tube to another, defining a pattern of inter-linkage. Using a model field, in which flux tubes are represented as point magnetic charges, it is possible to quantify this inter-linkage. If the coronal field were current free then motions of the magnetic features would change the inter-linkage through implicit (vacuum) magnetic reconnection. Without reconnection the conductive corona develops currents to avoid changing the flux linkage. This current forms singular layers (ribbons) flowing along topologically significant field lines called *separators*. Current ribbons store magnetic energy as internal stress in the field; the amount of energy stored is a function of the flux tube displacement. To explore this process we develop a model called the *minimum current corona* (MCC) which approximates the current arising on a separator in response to displacement of photospheric flux. This permits a model of the quasi-static evolution of the corona above a complex active region. We also introduce flaring to rapidly change the flux inter-linkage between magnetic features when the internal stress on a separator becomes too large. This eliminates the separator current and releases the energy stored by it. Implementation of the MCC in two examples reveals repeated flaring during the evolution of simple active regions, releasing anywhere from 10^{27}–10^{29} ergs, at intervals of hours. Combining the energy and frequency gives a general expression for heat deposition due to flaring (i.e. reconnection).

1. Introduction

Solar flares are dramatic bursts of energy from the Sun's chromosphere and corona. The build-up and release of energy in a flare has been the subject of extensive study leading to the prevailing view that energy is stored as stress in the coronal magnetic field prior to release (Gold and Hoyle 1960, Van Hoven *et al.* 1980). This viewpoint holds that slow motions of the photosphere cause stresses to accumulate in the coronal magnetic field. During this period electric fields are small and time scales are long so magnetohydrodynamics (MHD) is generally applicable, frequently in the equilibrium (quasi-static) limit. A flare is a rapid conversion of stored magnetic energy into accelerated particles, heat or bulk plasma motion. The detailed mechanism of energy conversion has been the subject of separate investigations focusing on local portions of the corona where significant electric fields have developed.

Studies of energy build-up typically focus on changes to a particular magnetic configuration, e.g. a magnetic arcade (Low 1977) or semi-toroidal loop (Hood and Priest 1979) terminating in a single flare event. While the geometries treated in this way are generally simple, the actual solar corona is quite complex, arising as it does from an assembly of isolated magnetic features at the photosphere. These features have been interpreted as the "tops" of slender flux tubes which have emerged from the dynamo layer below (Parker 1955, D'Silva and Choudhuri 1993, Fan *et al.* 1994, Caligari *et al.* 1995). The complex coronal field is continuously evolving, presumably due to the motions of the underlying flux tubes. This relatively slow evolution is accompanied by sporadic flares which can span a wide range of energies.

This paper presents a model, called the *minimum current corona* (MCC), for the build-up of magnetic energy in a three-dimensional corona of arbitrary geometry. The MCC model is based on the coronal flux linkage between different magnetic features. As Sweet (1958b) pointed out, treating the magnetic features as discrete objects (i.e. point magnetic charges) defines precise boundaries in the pattern of field line linkages, termed *separatrices* and *separators*. We show that motions of magnetic features cause stress in the coronal field to be focused at these boundaries giving rise to current singularities (current sheets) along the separators. This stress can be released only through an electric field parallel to the separator field line: magnetic reconnection. By adopting a primitive, *ad hoc* model for reconnection ("stick-slip") the MCC model can also account for the corona's continuing evolution and sporadic flaring.

Recently Sweet's topological picture of coronal linkage has been quantified in a series of models, here referred to as *magnetic charge topology* (MCT), proposed in seminal form by Baum and Bratenahl (1980) and subsequently explored by numerous authors (Gorbachev and Somov 1988, Priest and Forbes 1989, Somov 1992, Lau 1993, Démoulin *et al.* 1994a, Parnell *et al.* 1994). Applications of MCT in modeling flaring active regions (Machado *et al.* 1983, Mandrini *et al.* 1991, Démoulin *et al.* 1993, Brown *et al.* 1994, Bagalá *et al.* 1995) have revealed a correspondence between the separatrix/separator locations and the observed signatures of flares. This correspondence provides observational evidence suggesting that magnetic reconnection plays a crucial role in solar flares. The MCT model does not, however, include currents and so cannot model the energy stored in the fields or released in the flares. The MCC model developed here introduces currents and energetics to the MCT models.

The next section of this paper reviews the fundamentals of MCT models for coronal fields, and introduces the effects of flux tube motion. The MCC model is presented in §3, along with a brief account of current sheet formation. The stick-slip reconnection model is added in §4 and an example of coronal evolution is computed. In this example the single separator field line serves as the site of coronal current and energy deposition, resulting in intermittent brightening during its evolution. Section 5 considers a second example containing two separators which interact through the effect of mutual inductance. This opens the possibility of sympathetic flaring in which reconnection on one separator can trigger it on the other. When this occurs both loops brighten simultaneously forming a Y-shaped coronal loop complex.

2. Magnetic Charge Topology

2.1. Modeling coronal fields

The solar magnetic field changes form drastically in a narrow layer around the photosphere and chromosphere. Below this layer, in the convection zone, the magnetic field is confined to slender isolated strands (flux tubes) by much higher gas pressure ($\beta \gg 1$) and by rapid convective motions. The confining gas pressure is absent from the corona ($\beta \ll 1$) so the magnetic field expands to fill space in force-free equilibrium; there are no isolated flux tubes there. In the layer separating these two regimes the field "blossoms" from the confines of the flux tube into its space-filling form. This blossoming occurs within a layer called the magnetic canopy approximately 2000 km thick (Kopp and Kuperus 1968, Gabriel 1976, Giovanelli 1980, Giovanelli and Jones 1982).

A crude model of the blossoming magnetic field is offered by a magnetic point charge q_i on a conducting plane at $z = 0$ (see Figure 1). Although the conducting plane represents the entire canopy layer, henceforth it will simply be called the photosphere. Above the photosphere the magnetic field is directed radially away from the charge. Implicit in this picture is a horizontal surface current flowing just beneath the magnetic canopy (Sweet 1958b). The resulting Lorentz force compensates a discontinuous drop in plasma pressure across the interface separating regions with and without field.

A collection of emergent flux tubes is modeled by summing the contributions from magnetic point charges (Figure 1). A current-free coronal field can be written by analogy to electrostatics

$$\mathbf{B}(\mathbf{x}) = \sum_i \frac{\psi_i}{2\pi} \frac{\mathbf{x} - \mathbf{x}_i}{|\mathbf{x} - \mathbf{x}_i|^3} \quad . \tag{1}$$

where $\mathbf{x}_i$ is the location of charge i on the photosphere ($z_i = 0$) and $\psi_i = 2\pi q_i$ is its flux. This field applies only to the corona, but extending Equation (1) to the domain below (Schmidt 1964) results in a *mirror corona*, formally eliminating the photospheric surface current from consideration. Mirror coronae for general fields are found by reflecting the field in the corona according to a simple prescription. At the reflected point $(x, y, z) \rightarrow (x, y, -z)$ the magnetic field and vector potential are $(B_x, B_y, B_z) \rightarrow (B_x, B_y, -B_z)$ and $(A_x, A_y, A_z) \rightarrow (-A_x, -A_y, A_z)$. Currents in the corona give rise to image currents in the mirror corona $(J_x, J_y, J_z) \rightarrow (-J_x, -J_y, J_z)$. The reflected electric field $(E_x, E_y, E_z) \rightarrow (-E_x, -E_y, E_z)$ cancels the tangential component at the conducting photosphere. The electrostatic potential is $\phi \rightarrow -\phi$ so the photosphere is an equipotential: $\phi(x, y, z=0) = 0$. Note that the photosphere is modeled as a conductor because it resists the penetration of coronal flux, and not because of its intrinsic conductivity (which is comparatively low).

This model involves two major approximations: the corona is current-free and its sources can be represented by point charges. The first approximation, a current-free (or potential) field, has long been used to extrapolate measured photospheric fields into the corona (Schmidt 1964, Altschuler and Newkirk 1969), but it is the least accurate in a series of models which also include force-free fields with uniform and varying field line torsion (Nakagawa and Raadu 1972, Mikic and McClymont 1994). This relative inaccuracy is not a serious limitation for MCT models since their focus, the topology of the field, is quite robust. When used for general field modeling, potential fields are usually extrapolated from the continuous distribution of photospheric flux, inferred from a magnetogram rather than from a set of point charges. Point charges, while less accurate, are used in MCT models because they endow the field with a definite topology: each field line ends at two particular charges.

When used to model magnetograms charges are often placed *below* the photosphere ($z_i < 0$) and their depths adjusted along with their horizontal locations to best fit the measured field $B_z(x, y, z=0)$ (Démoulin *et al.* 1993). The depth of the charges does not affect the field line topology; thus we choose to place the charges exactly at $z = 0$ in order to make the photosphere the top of every flux tube. This makes it necessary to refer B_z to some surface $z = z_v > 0$ for the purpose of visualization.

2.2. Field line topology

The linkage between tubes (charges) is found by tracing magnetic field lines in Equation (1). A field line $\mathbf{r}(s)$ is traced by integrating the field line equation

$$\frac{d\mathbf{r}(s)}{ds} = \frac{\mathbf{B}[\mathbf{r}(s)]}{|\mathbf{B}[\mathbf{r}(s)]|} \tag{2}$$

beginning at some initial point $\mathbf{r}(0)$. As an example, consider the field from two parallel magnetic bipoles (Sweet 1958b, Baum and Bratenahl 1980). This field can be modeled using two positive and two negative charges ($N1$, $N2$, $S1$ and $S2$) placed on the photosphere in the configuration shown in Figure 2. All charges are given the same magnitude, which we will denote ψ_0. With a few notable exceptions, field lines originate at a positive charge, either $N1$ or $N2$, and end at a negative charge, either $S1$ or $S2$. This allows coronal field lines to be grouped into four domains according to their termini. Between these domains are surfaces called separatrices. These surfaces are formed from field lines beginning or ending at a magnetic null point rather than a charge (Sweet 1958b).

A null is a point where all components of the vector $\mathbf{B}$ vanish. In the vicinity of a null $\mathbf{x}_0$ the magnetic field can be expanded

$$\mathbf{B}(\mathbf{x}) = \mathrm{M} \cdot (\mathbf{x} - \mathbf{x}_0) \ + \ \ldots \quad . \tag{3}$$

For a force-free field the matrix M will be symmetric and will therefore have three real eigenvalues $m_1 \leq m_2 \leq m_3$ and orthonormal eigenvectors, $\hat{\mathbf{e}}_s$. The field divergence at $\mathbf{x}_0$ is

$$\nabla \cdot \mathbf{B} = \mathrm{Tr}\{\mathrm{M}\} = \sum_s m_s = 0 \quad ,$$

so in general there is at least one positive and one negative eigenvalue (Cowley 1973, Yeh 1976). In this sense all nulls in a force-free field are hyperbolic. The sign of the intermediate eigenvalue can be used to classify the null (Cowley 1973): a positive (negative) intermediate eigenvalue defines a null of type-B (type-A). The degenerate case in which the intermediate eigenvalue vanishes would only occur for very special arrangements of charges and need not be considered in general.

Our example contains one magnetic null of each type. The locations of these nulls, $\mathbf{x}_A$ and $\mathbf{x}_B$, are found numerically and shown in Figure 2. Symmetry dictates that these nulls lie at $z = 0$. Field lines originating at $\mathbf{x}_B$ form a separatrix surface called Σ_B. At $\mathbf{x}_B$ this surface is tangent to the plane spanned by $\hat{\mathbf{e}}_2^B$ and $\hat{\mathbf{e}}_3^B$. The surface separates field lines originating at $N1$ from those originating at $N2$ (note that Σ_B is composed of the only field lines which originate at neither charge). The intersection of Σ_B with the visualization surface z_v is shown by a solid curve in Figure 2. Similarly, the separatrix Σ_A divides field lines ending in $S1$ from those ending in $S2$; its intersection with z_v is shown by a dashed line. Together Σ_B and Σ_A divide the corona into four domains of topologically distinct field lines, labeled $N1 - S1$, $N2 - S2$, $N2 - S1$ and $N1 - S2$ (see Figure 2). (More thorough analyses of this configuration are given by Baum and Bratenahl [1980] and Gorbachev and Somov [1988]).

The surfaces Σ_A and Σ_B intersect each other along one field line above the photosphere. This field line is called the *separator* and is designated σ_{21} in our example. The separator begins at $\mathbf{x}_B$ and ends at $\mathbf{x}_A$, since it is simultaneously a member of Σ_A and Σ_B. Appendix A presents an algorithm for locating and tracing the separator field line. A second separator $\bar{\sigma}_{21}$ goes from $\mathbf{x}_B$ to $\mathbf{x}_A$ through the mirror corona ($z < 0$) along a reflection of σ_{21}. Together the field lines σ_{21} and $\bar{\sigma}_{21}$ form a closed loop called a separator loop (Longcope and Cowley 1996). Integrating the magnetic flux across a surface $\mathcal{S}_{21}$ bounded by the separator loop gives Ψ_{21}, the net flux linking $N2$ to $S1$ through the corona:

$$\int_{\mathcal{S}_{21}} \mathbf{B}\cdot d\mathbf{S} = \oint_{\sigma_{21}\cup\bar{\sigma}_{21}} \mathbf{A}\cdot d\mathbf{l} = 2\Psi_{21} \quad . \tag{4}$$

We will adopt the convention that integration over a separator loop proceeds from the B-null to the A-null (i.e. parallel to $\mathbf{B}$) above the photosphere and then back from A to B (anti-parallel to $\mathbf{B}$) below the photosphere. Integration along the numerically determined separator (see Appendix A) yields $\Psi_{21} \simeq 0.32\,\psi_0$ for the configuration shown in Figure 2. The remaining flux from $N2$ must go to $S2$, so $\Psi_{22} = \psi_0 - \Psi_{21} = 0.68\,\psi_0$. The other fluxes, $\Psi_{11} = \Psi_{22}$ and $\Psi_{12} = \Psi_{21}$, follow from similar arguments.

2.3. Changing topology from moving flux tubes

The partitioning of flux between the various domains follows from the locations of the flux tubes (charges) which define the coronal field (1). If these tubes were to move (i.e. if $\mathbf{x}_i$ were to change) the coronal field would change and so would the apportionment of coronal flux. To demonstrate this we will define an evolution, to be called the *shear scenario*, in which the two bipoles move past one another in a continuous shearing displacement (see Figure 3). The distance between the poles of each bipole, denoted d, will be held fixed as will the distance between their axes, Δy. Following Baum and Bratenahl we will take $\Delta y = d$. During their shearing motion, the parameter Δx will begin at zero (bipoles aligned) and increase. Figure 2 represents the instant where $\Delta x = d$. The choices $d = 30,000$ km and $\psi_0 = 3\times 10^{20}$ Mx represent a small pair of bipoles. Rapid motion, as sometimes occurs during the emergence of new flux, corresponds to $d(\Delta x)/dt = 300\,\mathrm{m/sec}$.

As the flux tubes (charges) move, the coronal magnetic field must change accordingly. We will begin by assuming that the corona remains current-free, so that Equation (1) can be used to find the null points, $\mathbf{x}_A$, $\mathbf{x}_B$, and the separator σ_{21}. Figure 4 shows the length of the separator L and the enclosed flux Ψ_{21} as functions of Δx. When the bipoles are aligned ($\Delta x = 0$) the field is symmetric about $y = 0$ and no field lines cross between bipoles. This leads immediately to the result $\Psi_{21} = 0$: flux leaving $N2$ connects only to its companion $S2$ and similarly for $N1$ and $S1$. Initially, $N2$ and $S1$ approach each other causing Ψ_{21} to increase with Δx. They are closest at $\Delta x = d$, however, the shared flux, Ψ_{21}, reaches its maximum, $\Psi_{21} \simeq 0.33\,\psi_0$, at $\Delta x \simeq 1.33\,d$. Thereafter, the two bipoles become increasingly isolated and the shared flux tends to zero as $\Delta x \to \infty$. Once $\Delta x \gg \Delta y$ the misalignment of axes can be ignored and the problem approaches an axisymmetric one of two co-axial dipoles with moments $\mu = q_0 d$. In the axisymmetric case the separator goes over to a ring of nulls (Longcope and Cowley 1996) with circumference $2L = \sqrt{2}\pi\,\Delta x$ and enclosing flux $2\Psi_{21} = \psi_0(8/3\sqrt{3})\,d/\Delta x$. For reference these limiting cases are also shown in Figure 4.

This example can be interpreted to show that some reconnection is necessary if the corona is to remain current-free as we have assumed. Here the term reconnection means a re-mapping of field-line footpoints. For example, some of the field lines connecting $N2$ to $S2$ must be re-mapped to connect $N2$ to $S1$ for Ψ_{21} to increase. The rate at which flux must be re-mapped is given by $\dot{\Psi}_{21}$. Time differentiating Equation (4) leads to a version of Faraday's law

$$\dot{\Psi}_{21} = \tfrac{1}{2} \oint\limits_{\sigma_{21} \cup \bar{\sigma}_{21}} \partial_t \mathbf{A} \cdot \mathrm{d}\mathbf{l} = -c \int\limits_{\sigma_{21}} E_{\parallel} \, \mathrm{d}l \quad , \tag{5}$$

where we have used the fact that the electrostatic potential is constant on $z = 0$. Taking the values specified above for ψ_0 and d gives a maximum integrated electric field of 10^7 Volts, or an average of $\langle E_{\parallel} \rangle \simeq 0.1\,\mathrm{V/m}$ along the separator.

Thus an electric field parallel to the separator is required to change the flux Ψ_{21} linking $N2$ to $S1$. This could be called a voltage drop between $\mathbf{x}_B$ and $\mathbf{x}_A$, but it is actually one leg of an inductive loop voltage (A and B are always at the same electrostatic potential ϕ). If the remaining leg were $\bar{\sigma}_{21}$ then the full loop voltage would be twice as large, reflecting the additional flux from the mirror corona. On the other hand, completing the loop just beneath the photosphere adds nothing to the loop voltage since the horizontal electric field must vanish there. Thus, because we have assumed that flux cannot cross the photosphere, any inductive electric field must appear in the corona.

In a conducting plasma with local velocity $\mathbf{v}$ the electric field is given by Ohm's law

$$\mathbf{E} = -\frac{1}{c}\mathbf{v} \times \mathbf{B} + \eta \mathbf{J} \quad , \tag{6}$$

where η is the plasma's resistivity. This expression yields $E_{\parallel} = 0$ in our current-free corona since the first term on the rhs of Equation (6) is perpendicular to $\mathbf{B}$ and the second vanishes by assumption ($\mathbf{J} = 0$). It should also be noted that in the limit of vanishing resistivity, $\eta = 0$, $E_{\parallel}$ must vanish even in the presence of current ($\mathbf{J} \neq 0$). There are therefore two alternatives for the coronal plasma: either it remains current-free by some mechanism which gives rise to a substantial $E_{\parallel}$ (reconnection) or it develops currents in order to prevent the flux Ψ_{21} from changing. It is noteworthy that a parallel electric field would lead to some of the effects associated with solar flares, such as the acceleration of charged particles to high energies. This suggests that signatures of particle acceleration should appear near the separator field line, and indicate a departure from Equation (6).

A series of observational studies have been conducted to test this hypothesis (Mandrini *et al.* 1991, Démoulin *et al.* 1993, Démoulin *et al.* 1994b, Bagalá *et al.* 1995). In these studies point charges are used to fit magnetograms from flare-productive active regions and separators are calculated from the resulting MCT. Observations of the flare in various wavelengths can then be referred to features in the MCT model. These are found to have a decided correlation with separatrix and separator locations. In particular, $H\alpha$ kernels are located where separatrices intersect the photosphere (Mandrini *et al.* 1991, Démoulin *et al.* 1993) and radio, X-ray and UV emission at higher points along the separator (Démoulin *et al.* 1994b, Bagalá *et al.* 1995). One would not expect locations to correspond perfectly for several reasons, including the approximate nature of the magnetic field extrapolation. The degree to which they do agree, however, suggests a relationship between separator lines and flaring. The logical implication is that flares are the result of magnetic reconnection occurring along the separator field line.

In summary, a current-free (vacuum) model of the coronal field (Equation [1]) can be used to identify the topology of coronal magnetic fields. This topology can be completely characterized by its separator field line σ_{21} and the magnetic flux enclosed by it. Using the vacuum field to calculate this flux leads to a value hereinafter denoted $\Psi_{21}^{(\mathrm{v})}$, which depends only on the configuration of charges. Moving the charges causes $\Psi_{21}^{(\mathrm{v})}$ to change in a known way, e.g. $\Psi_{21}^{(\mathrm{v})}(\Delta x)$ in Figure 4b. Changing the flux inside σ_{21}, however, requires a substantial electric field, $E_{\parallel}$, inconsistent with Ohm's law and a vacuum field.

3. The Minimum Current Corona

To resolve this inconsistency we must modify our model to admit the presence of coronal current in response to flux tube motion. Our model will continue to be a quasi-static one, so the current-carrying field must be in force-free equilibrium. Recently Longcope and Cowley (1996) studied the quasi-static evolution of a magnetic field containing a separator loop. They found that the field evolves into a series of equilibrium configurations containing closed current sheets along the separator loop: *current ribbons*. The shape of the ribbon is determined by local force balance, and by detailed topological constraints. Specifically, there are no field lines winding around the current, since they would have no counterparts in the initial current-free configuration. It is for this reason that the current must form a flat ribbon. A two dimensional analog of this is the development of a current sheet by distorting an X-point (Syrovatskii 1971). In this analogy the separator field line plays the role of the X-point.

The resulting force-free equilibrium is current-free everywhere except along the separator field line. In particular, all field lines which emerge from flux tubes remain current-free. The separator current is necessary to hold fixed the partitioning of flux among the different flux tubes. The flux partitioning, quantified by the separator flux Ψ_{21}, forms a constraint which the equilibrium coronal magnetic field must satisfy. Aside from the requirement that B_z match Equation (1) at the photosphere, the flux partitioning constraint is the *only* constraint applied here. In particular, field lines are unconstrained within each domain and thus can reorganize themselves to achieve their lowest energy state: i.e. current-free. We therefore believe that our model represents the corona with the minimum permissible current, and will therefore be called the *minimum current corona.*

When working with the separator and its current I_{21} it is most convenient to complete the circuit through the mirror corona, along $\bar{\sigma}_{21}$, enforcing by symmetry the condition $B_z = 0$ at the photosphere, except at the charges. This is *not*, however, the physical path taken by the return current. As in a textbook magnetostatics problem the image current on $\bar{\sigma}_{21}$ actually represents a current flowing over a broad region on the surface ($z = 0$) just below the coronal magnetic field. Recall that there is already a substantial surface current flowing there from the potential field. The return current flowing between A and B will be a perturbation to this. Furthermore, since the separator line ends at the photosphere, and does not enter a flux tube, the return current does not cross field lines. By contrast, currents carried along flux tubes must either cross field lines or close through the whole length of the subsurface flux tube (Melrose 1995).

The current in the ribbon flows parallel to field lines which take the place of the original separator. The flux inside these field lines, and therefore inside the current ribbon, will be denoted Ψ_{21}. This flux includes contributions from the vacuum field and from the self-flux of the current I_{21}

$$\Psi_{21} = \Psi_{21}^{(\mathrm{v})}(\Delta x) + \Psi_{21}^{(\mathrm{cr})}(I_{21}) \quad . \tag{7}$$

Hereafter we will assume that the corona is ideal ($\eta = 0$) and therefore that the flux Ψ_{21} cannot change ($\dot{\Psi}_{21} = 0$) in spite of the current. We will return to this point in Section 6 to show that the assumption is a good one, given the high conductivity of the corona.

Beginning with a configuration of charges for which the corona is current-free, call it $\Delta x = \Delta x_0$, the flux must remain fixed at the value

$$\Psi_{21} = \Psi_{21}^{0} \equiv \Psi_{21}^{(\mathrm{v})}(\Delta x_0) \quad . \tag{8}$$

As Δx increases, $\Psi_{21}^{(\mathrm{v})}(\Delta x)$ changes according to Figure 4b, and $\Psi_{21}^{(\mathrm{cr})}(I_{21})$ must change in such a way as to keep the right-hand side (rhs) of Equation (7) constant. We can therefore solve for the current I_{21} by inverting the function $\Psi_{21}^{(\mathrm{cr})}(I_{21})$.

The precise functional relationship between I_{21} and $\Psi_{21}^{(\mathrm{cr})}$ will be quite complex, depending on the interaction of the current and the vacuum field. Our purposes will be adequately served by an approximate form of this relation, derived in Appendix B. Assuming that the current distorts the path of the separator only locally, the current-flux relation can be cast in terms of the length L of the separator and a quantity with units of current which we denote $I_{21}^{\star}$. The latter principally involves gradients of the vacuum magnetic field (e.g. $\partial B_x/\partial x$) perpendicular to the separator, averaged over the separator (see Equation [B9] in Appendix B for the exact definition). Since this quantity is computed from the vacuum field alone it is not related to any actual current. The quantities L and $I_{21}^{\star}$ can be combined into a characteristic flux

$$\Psi_{21}^{\star} \equiv \frac{L I_{21}^{\star}}{c} \quad , \tag{9}$$

in terms of which the current-flux relation takes the form (Equation [B10])

$$\Psi_{21}^{(\mathrm{cr})}(I_{21}) = \Psi_{21}^{\star} \frac{I_{21}}{I_{21}^{\star}} \ln\left[256 e^{-3} \, \frac{I_{21}^{\star}}{|I_{21}|} \right] \; \equiv \; \Psi_{21}^{\star} \, \Lambda(I_{21}/I_{21}^{\star}) \quad . \tag{10}$$

This algebraic relationship summarizes the inductive properties of the current ribbon. The differential inductance of the ribbon

$$\mathcal{L} = \frac{1}{c}\frac{d\Psi_{21}^{(\mathrm{cr})}}{dI_{21}} = \frac{L}{c^2}\ln\left[256e^{-4}\frac{I_{21}^{\star}}{|I_{21}|}\right] \quad , \tag{11}$$

depends on the current it carries. A sheet of length L and width w has an inductance $\mathcal{L} \sim 2L\ln(L/w)$ (Somov 1992). The current deforms its own magnetic field locally, leading to a relationship

$$I_{21} \sim B'_{\perp}w^2 \quad , \tag{12}$$

where $B'_{\perp}$ is a coefficient expressing the gradients of the external (vacuum) magnetic field perpendicular to the separator (e.g. $\partial B_x/\partial x$). This relation gives the inductance its $\ln|I_{21}|$ dependence (Longcope and Cowley 1996). The constant of proportionality between w^2 and I_{21} defines $I_{21}^{\star}$. Appendix B gives an explicit expression for $I_{21}^{\star}$ based on a more detailed calculation. Its actual value is not terribly critical since it appears only inside the logarithm in Equation (10).

The procedure above will be used to approximate the self-flux of a current ribbon. It is most accurate in the limit of vanishing current, $|I_{21}| \ll I_{21}^{\star}$, and only applies to cases where the cross section of the separator resembles a two-dimensional X-point. These assumptions are introduced to formulate an explicit flux-current relation which is local in the sense that it depends only on the field in the neighborhood of the separator. There are some circumstances where the assumptions fail and a local current-flux relationship may be impossible. These cases, referred to as "structurally unstable" in Appendix B, occur when some portion of the separator ribbon violates the assumption of local two-dimensionality. At such points, which typically occur over a short portion at the top of the separator, a local relationship between current and sheet width, like Equation (12), does not exist. A global relationship between the current I_{21} and induced flux $\Psi_{21}^{(\mathrm{cr})}$ must still exist, in spite of this violation; however, we cannot presently say what form this relationship would take. Pending a more thorough understanding of three-dimensional current sheets we will adopt the expedient measure of using expression (10) with $I_{21}^{\star}$ taken to be some default value. Choosing this default value to be small will minimize the effect of this measure.

The inductive properties of the separator σ_{21} are found from numerical integration along the separator for each configuration Δx (see Figure 5). The separator is structurally unstable over the range $\Delta x < 0.53\,d$, so $I_{21}^{\star}$ is assigned the default value $0.01\,c\psi_0/d$ there. Structural instability is a function of the photospheric configuration, and not the current or the choice of vacuum state Δx_0. The lack of structural stability for small Δx could result from the singular nature of the configuration $\Delta x = 0$. This singularity occurs because the system is reflectionally symmetric about $y = 0$ implying that Σ_A and Σ_B coincide exactly, rather than intersecting along a unique separator. In the opposite limit, $\Delta x \to \infty$, the system approaches axisymmetry (Longcope and Cowley 1996) for which the analytic solution $I^{\star}_{21}/c \simeq 0.058\,\psi_0/(\Delta x)^2$ obtains. Finally, it is worth noting that the maximum of $\Psi^{\star}_{21}$, at $\Delta x \simeq 1.2\,d$, is only 20% of Ψ_{21} at its maximum.

The flux-current relationship, Equation (10), is used to find I_{21} from the requirement of frozen-flux (Equation [8])

$$\frac{\Psi^{(\rm v)}_{21}(\Delta x) - \Psi^0_{21}}{\Psi^{\star}_{21}} \equiv \frac{\Delta\Psi_{21}}{\Psi^{\star}_{21}} = -\Lambda(I_{21}/I^{\star}_{21}) \quad . \tag{13}$$

Inverting the function $\Lambda(x) = -x\ln(|x|/12.745)$, from Equation (B10), allows I_{21} to be found as a simple function of the bipole displacement Δx. In the regime $\Delta x \leq 1.33\,d$, where $\Psi^{(\rm v)}_{21}$ increases, the lhs of this equation will be positive and increasing. This implies an increasingly negative current, which by our convention, means a current flowing through the corona from A to B (anti-parallel to $\mathbf{B}$) and generating a self-flux directed from $S1$ toward $N2$. This is the correct sense to screen $S1$ from $N2$ as they approach each other.

The magnetic field with current has higher energy than the corresponding vacuum field. The additional energy due to the current can be calculated as the energy of an inductor (Longcope and Cowley 1996)

$$\Delta\mathcal{E}(I_{21}) = \frac{1}{c}\int_0^{\Psi^{(\rm cr)}_{21}} I(\Psi)\,{\rm d}\Psi = \frac{L}{2c^2}\,I^2_{21}\,\ln[\,256e^{-7/2}\,I^{\star}_{21}/|I_{21}|\,] \quad . \tag{14}$$

This energy difference, termed non-potential energy, is not localized to the current ribbon itself; it takes the form of enhanced magnetic field strengths throughout the corona.

Expression (14) gives the difference between the energy of the coronal magnetic field with and without current. In fact, the total magnetic field energy is formally infinite since it includes point charges. (This would not be the case for $z > z_v$.) Since the self-energy of the point charges does not change, all energy differences are finite. This is true of the difference between field with and without current and is also true of the difference between potential fields from differing charge arrangements. The latter energy difference can be written as the change in the "interaction" energy

$$\mathcal{E}_0 = \frac{1}{(4\pi)^2}\sum_{\substack{i,j\\ i\neq j}} \frac{\psi_i\psi_j}{|\mathbf{x}_i - \mathbf{x}_j|} \quad , \tag{15}$$

for different configurations. The power required to move the flux tubes (charges) is the derivative of the combined energy $\mathcal{E}_0 + \Delta\mathcal{E}$. This power must be supplied by the flux tubes themselves, or by whatever forces would move them.

4. Stick-slip Reconnection

There is much evidence to suggest that coronal activity, such as flaring, occurs when field aligned electric fields develop in the corona. This releases substantial energy which is stored prior to the flare as non-potential magnetic energy. Storing non-potential energy requires that the corona, at least for some time, support current density without an accompanying electric field (i.e. that it be highly conductive). On the other hand, releasing that energy rapidly (impulsive flare bursts last just a few Alfvén times) requires very large electric fields. In this gross sense the corona seems to change its conductivity very abruptly.

An accepted theory of how the corona changes its conductivity in a solar flare has yet to be found. Our model does not concern itself with the details of this process, but rather its consequences. We will therefore postulate only that stresses arising from flux tube motions are released abruptly by flares, which then remap the field lines between flux tubes. Toward this end we propose an *ad hoc* "stick-slip" reconnection model to implement flaring. This assumes the corona to be a perfect conductor, holding fluxes fixed at each separator. As a result current I_{21} develops along the separator loop in response to flux tube motion. It also assumes that some limit exists to this build-up. For concreteness, we will express this limit as a *threshold* θ on the ratio $|I_{21}|/I^{\star}_{21}$, although this is not the only quantity on which a limit could conceivably exist. When this threshold is crossed, a "flare" is triggered, by which we mean the onset of an electric field, $E_{\parallel}$, that is capable of changing the flux inside σ_{21}, thus reducing $\Delta\Psi_{21}$. Here we will make a second assumption: the flare will result in *complete* reconnection, $\Delta\Psi_{21} \to 0$. That is to say once the flare is triggered, the corona is returned to its vacuum state. While it seems reasonable to expect $\theta \ll 1$ we can presently say no more about its value.

Reducing the magnitude of $\Delta\Psi_{21}$ permits the coronal field to relax to a lower energy state. In our model, which only represents equilibrium fields, this happens instantaneously. In reality, however, the change propagates through the corona as a disturbance of the field, accompanied by plasma motion. If magnetic energy is converted *directly* at the point of reconnection the disturbance must transport the energy, as a Poynting flux, to the separator from throughout the corona. Thus, within the time taken for an Alfvén wave to cross the active region, it is possible in principle to liberate all the stored energy (Melrose 1992). Our model, however, cannot describe how or where the energy conversion takes place. For instance, it is possible for magnetic energy to be converted to bulk kinetic energy, such as outflow jets. On the other hand, if the plasma remained eternally in motion after a flare then the corona would never again return to equilibrium. Since the real corona appears quite stationary most of the time, we will assume that large-scale bulk motion ultimately dies away. Thus all of the non-potential energy will eventually be converted to heat or radiation and we can call $\Delta\mathcal{E}$ the total flare energy.

As mentioned in Section 2.3, we will consider two small bipoles, each with flux $\psi_0 = 3 \times 10^{20}$ Mx and with poles separated by $d = 30,000\,\mathrm{km}$. The shearing will arise through rapid evolution whose relative velocity is $d(\Delta x)/dt = 300\,\mathrm{m/sec}$. Finally, we will adopt a threshold value $\theta = 0.15$. These choices result in the time history shown in Figure 6. Each dotted curve in Figure 6a is the complete solution for $I_{21}/I^{\star}_{21}$ from solving Equation (13) for a single value of Ψ^0_{21}. A flare occurs when this curve crosses $\pm\theta$; I_{21} is then reset to zero, Ψ_{21}^0 is reset to the new value of Ψ_{21} and a new dotted curve is followed. That is, flux Ψ_{21} remains constant ($=\Psi_{21}^0$) between flares following $\Psi_{21}^{(\mathrm{v})}(t)$ in a stair-step fashion (Figure 6c). Each step represents a transfer of $\simeq 10^{19}$ Mx of flux between footpoints, and across the separator. If each transfer occurred within 100 seconds the voltage drop along σ_{21} would be 10^9 volts. During these instants the differential inductance of the current ribbon (Equation [11]) is $\simeq 30$ Henrys, and the net currents are $\simeq 3\times 10^9$ Amps.

The first twenty hours are the most active, involving seven flares, each releasing $\simeq 10^{27}$ ergs. Four small flares occur in the regime of structural instability where the current-flux relationship is actually not known; the three larger flares are from more accurately modeled regimes. Were a smaller default value of $I_{21}^\star$ used in the regime of structural instability the frequence of flaring would increase while the amplitude would decrease. The energies and frequencies in the other portion are typical of events called transient brightenings (Shimizu *et al.* 1992) which are possibly related to microflares. During this time the potential energy $\mathcal{E}_0$ (not shown) drops by $\simeq 5\times 10^{28}$ to its minimum value. As the bipoles become more widely separated, the activity diminishes.

When a flare is triggered the non-potential energy, amounting to $\simeq 10^{27}$ ergs in this example, is released abruptly within a region probably along the separator field line. Whether the energy takes the form of heat directly, or accelerated particles impacting the chromosphere, the energy release would result in the evaporation of chromospheric material into the loop. This would, in turn, increase the luminosity along the whole field line. In short, a coronal loop at or near the separator would appear to brighten abruptly in UV and X-ray images. After energy release, the loop will gradually cool and drain, fading from view until the next event. While none of these details enter our model, they are the implicit byproduct of the reconnection event. This leads to a picture in which coronal loops occasionally brighten and fade, similar to observations of transient brightenings made in soft X-rays.

The frequency with which events occur, and the energy each releases, is determined by the choice of threshold θ. Smaller values result in smaller, but more frequent flares. The non-potential energy stored at the threshold is

$$\Delta\mathcal{E}_\theta = \frac{\theta^2}{2c} I_{21}^\star \Psi_{21}^\star \, \ln(256 e^{-7/2}\,\theta^{-1}) \quad . \tag{16}$$

The interval between flares is the time required for $|\Delta\Psi_{21}|$ to increase from zero to $\Psi_{21}^\star\Lambda(\theta)$, estimated to be

$$\Delta t \simeq \frac{\Psi_{21}^\star\Lambda(\theta)}{|\dot{\Psi}_{21}^{(\mathrm{v})}|} \quad . \tag{17}$$

Smoothing over the impulsive character of the flares we can write an average power dissipation

$$\bar{P} = \frac{\Delta\mathcal{E}_\theta}{\Delta t} \;\simeq\; \theta\left|\frac{d(\Delta x)}{dt}\right| \frac{1}{2c} I_{21}^\star \left|\frac{d\Psi_{21}^{(\mathrm{v})}}{d(\Delta x)}\right| \;\equiv\; \theta\,|v_{\Delta x}|\,|\bar{F}_{21}| \quad . \tag{18}$$

We have expressed the power in terms of a friction force $\theta\bar{F}_{21}$, which always has the sign opposite to $v_{\Delta x} = d(\Delta x)/dt$, but otherwise does not depend on velocity (like a kinetic friction in classical mechanics [Marion and Thornton 1988]). The factor $\bar{F}_{21}$ depends only on the magnetic configuration; for the initial portion of the shearing scenario ($\Delta x < 1.33\,d$) its value is $\bar{F}_{21} \simeq 0.025\,\psi_0^2/L^2$.

Both the friction force and the dissipated power depend on the choice of threshold. In this sense, the threshold θ expresses the energetic efficiency with which reconnection permits the motion of flux tubes. Modifying the stick-slip model so that only a fraction f of the flux is reconnected at each event (i.e. $I_{21} \rightarrow [1-f]\theta I_{21}^{\star}$) leads to a power which is *larger* by the factor $2-f$. This increase results from decreasing the interval Δt by f and decreasing the released energy by $1-(1-f)^2$. Thus less complete reconnection results in less efficient motions of the flux tubes.

5. A Case with Multiple Separators: Sympathetic Flaring

The example above contains two magnetic bipoles and a single separator field line. More complex configurations, with more flux tubes (charges) can contain more separators. To demonstrate this we consider a second example, the *emergence scenario*, which models the emergence of a small magnetic bipole inside a mature bipolar active region (see Figure 7). The active region consists of a single leading pole, S1, with flux ψ_1 and a fragmented following pole, N1 and N2, each of which has the flux $0.5\,\psi_1$. These are oriented horizontally (E-W) and have a fixed separation d. Inside this we introduce a second bipole, consisting of N0 and S0, each with flux $\psi_0 = 0.25\,\psi_1$ and oriented N-S. The separation between the poles, Δy, is increased to simulate flux emergence. Figure 7b shows successive locations of N0 and S0 (+'s) and the corresponding locations of the null points ($\triangle$'s). One B-type null (B2) occurs between N1 and N2, and moves very little. The other two null points, A and B1, occur in association with the emerging flux, and therefore move outward with the poles. During the initial stages of emergence the nulls separate as $|\mathbf{x}_A - \mathbf{x}_{B1}| \sim (\Delta y)^{1/3}$.

The additional pole has led to an additional null point in this scenario. Three null points admit the possibility of two separators, which are in fact present (see Figure 8). One separator (σ_{20}) links $B2$ to A, while the other (σ_{00}) links $B1$ to A. Their common origin at A leads to a Y-shaped configuration reminiscent of many flares and transient brightenings (Hanaoka 1994, Shimizu *et al.* 1994). The flux Ψ_{00} enclosed by σ_{00} links $N0$ to $S0$. At the instant of emergence ($\Delta y = 0$) the two poles are completely connected so $\Psi_{00} = -\psi_0$. The other separator, σ_{20}, encloses the flux linking $N2$ to $S0$. Initially, $\Psi_{20} = 0$ since $S0$ connects only to $N0$. Using this reasoning and the separator orientation convention we deduce that both $\Psi_{00}^{(\mathrm{v})}$ and $\Psi_{20}^{(\mathrm{v})}$ increase with Δy (i.e. $d\Psi^{(\mathrm{v})}/dt > 0$).

Changes in the vacuum fluxes through the various separator loops will induce currents as in the shearing scenario. In this case, however, there will also be interaction between the loops. A current on σ_{00} will give rise to a flux through the other separator loop (σ_{20}). Assuming this to be small enough to leave σ_{20} undisturbed the effect can be expressed using a mutual inductance $\mathcal{M}_{00,20}$ defined according to the Neumann formula (Jackson 1975)

$$\mathcal{M}_{\sigma,\sigma'} = \mathcal{M}_{\sigma',\sigma} = \frac{1}{2c^2} \oint_{\sigma\,\cup\,\bar{\sigma}} \oint_{\sigma'\,\cup\,\bar{\sigma}'} \frac{\mathrm{d}\mathbf{l}\cdot\mathrm{d}\mathbf{l}'}{|\mathbf{x}(l)-\mathbf{x}(l')|} \quad . \tag{19}$$

Because its denominator vanishes only at a single point in (l, l') space this integral converges even without accounting for the ribbon-like nature of the actual currents. The detailed equilibrium structure of two current sheets crossing each other has yet to be worked out.

The flux through separator σ includes a vacuum portion, a self-flux and fluxes from other separator currents

$$\Psi_\sigma = \Psi_\sigma^{(\mathrm{v})} + \Psi_\sigma^{(\mathrm{cr})}(I_\sigma) + \sum_{\sigma'\neq\sigma} c\mathcal{M}_{\sigma,\sigma'}\, I_{\sigma'} \quad . \tag{20}$$

Setting this expression equal to the fixed flux Ψ_σ^0 for that separator, gives the set of coupled nonlinear equations

$$-\frac{\Delta\Psi_\sigma}{\Psi_\sigma^\star} = \Lambda\Big(\frac{I_\sigma}{I_\sigma^\star}\Big) \; + \; \sum_{\sigma'\neq\sigma} \widetilde{\mathcal{M}}_{\sigma,\sigma'}\,\frac{I_{\sigma'}}{I_{\sigma'}^\star} \quad , \tag{21}$$

where $\widetilde{\mathcal{M}}_{\sigma,\sigma'} \equiv (cI_{\sigma'}^\star/\Psi_\sigma^\star)\,\mathcal{M}_{\sigma,\sigma'}$ is a dimensionless mutual inductance. Equations (21) are solved simultaneously to find the currents on each separator.

The inductive energy can be found by integrating $-c^{-1}I_\sigma\,\mathrm{d}(\Delta\Psi_\sigma)$ for all separators as each current is increased in turn,

$$\Delta\mathcal{E} = \sum_\sigma I_\sigma^2\frac{L_\sigma}{2c^2}\ln[256e^{-7/2}\,I_\sigma^\star/|I_\sigma|] \; + \; \sum_{\substack{\sigma,\sigma'\\ \sigma\neq\sigma'}} \tfrac{1}{2}\mathcal{M}_{\sigma,\sigma'}I_\sigma\, I_{\sigma'} \quad . \tag{22}$$

This contains the self-energy of each loop, which is always positive, and an interaction term which can be of either sign.

During evolution each current is compared to the threshold θ for reconnection. When one separator, say σ_*, exceeds this threshold a flare is triggered which reconnects all the flux necessary to eliminate the current on that separator: $I_{\sigma_*} \to 0$. This eliminates mutual flux contributions to all other separators, requiring their currents to change as well. To find the new currents Equations (21) must be solved anew on each separator except σ_*, but this time with $I_{\sigma_*} = 0$. The new currents can then be used in Equation (21) for $\sigma = \sigma_*$ to determine a new $\Psi_{\sigma_*}^0$; unlike the single-separator case this does not return to $\Psi_{\sigma_*}^{(\mathrm{v})}$ after a flare. Thus a flare on one separator, triggered when its own current exceeds the threshold, causes abrupt changes in the currents of all other separators through mutual inductance.

Following this procedure, it is possible for a flare on one loop to drive currents on nearby loops over their thresholds, thereby triggering sympathetic flares. We treat this event the same as the original flare, setting to zero all currents which have exceeded their thresholds, including I_{σ_*}. Then the remaining rows of Equation (21) (if there are any) are solved once more. Each time a subset is solved, it is possible for other flares to be triggered, and the process must be started again. Finally, when a solution is found with all currents below threshold, the fluxes Ψ^0_σ are found from the rows of Equation (21) corresponding to those separators which flared.

Figure 9 shows the result of applying this procedure to the emergence scenario. The pole $S1$ has a flux $\psi_1 = 2 \times 10^{21}$ Mx, while $N1$ and $N2$ each have fluxes of 10^{21} Mx, and the bipolar region has dimension $d = 100,000$ km. The emerging bipole has flux $\psi_0 = 5 \times 10^{20}$ Mx, its poles separate at a relative velocity of $300\,\mathrm{m/sec}$, and once again $\theta = 0.15$. The separator σ_{00}, surrounds the emerging bipole, and is the site of the most rapid changes causing five small flares ($\simeq 3 \times 10^{28}$ ergs) during the first ten hours. The dimensionless current on σ_{00} Figure (9a) changes rapidly in time, reaching the threshold quickly. During this time, the current on σ_{20} changes relatively little, however, the nearby flare induces additional current. This additional current is sufficient to induce sympathetic flares about every other time. As its length increases so does the self energy of σ_{00}; by $t = 12$ its solitary flare releases $\Delta\mathcal{E} \simeq 4 \times 10^{28}$ ergs. Sympathetic flares release energy from both loops, so they are systematically larger; the one at $t = 25$ hours is $\Delta\mathcal{E} \simeq 1.7 \times 10^{29}$ ergs. Note that it is possible for σ_{20} to trigger a sympathetic flare (as it does at $t = 34$) or to flare alone.

Roughly half of the time separator σ_{00} brightens alone, resembling the brightening in the shearing scenario. In a sympathetic flare, however, both loops would brighten almost simultaneously. The resulting configuration (e.g. Figure 8) resembles the kind of loop complex seen frequently in X-ray images.

6. Discussion

We have presented a new conceptual model, called the minimum current corona, for the quasi-static evolution of the coronal magnetic field in response to motions of photospheric features. By considering only the coronal interconnections between flux tubes, we have shown that coronal currents must occur during this evolution. This represents a kind of stress in the coronal field, caused by the motion of photospheric flux. The currents flow in ribbon-like structures which follow the separator magnetic field lines. The amount of current in a ribbon, and consequently the amount of stress in the field, can be calculated from the displacements of the footpoints.

The coronal field in our model is constrained only by conditions of flux interconnection, summarized by the fluxes Ψ_{ij}. Our constraints prevent the motion of field lines *between* domains, but allow free movement *within* a domain. This is different from a genuine line-tying constraint which would hold fixed the ends of each field line within a domain. True line-tying boundary conditions are difficult to envisage in a model with genuine point sources — to which "part" of a point is a field line tied? Thus, line-tied boundary conditions require a model for the flux tube's internal structure and for its internal motions, such as twisting. Satisfying these additional constraints leads to current within each domain, as well as between domains. These currents would not be sheets or ribbons, but would be continuous spatial distributions (Van Ballegooijen 1985, Antiochos 1987, Longcope and Strauss 1994). In reality, however, the self-consistent response of the magnetic flux tube to coronal stresses might not be most accurately modeled by tying the field lines to a perfectly rigid, perfectly conducting point-charge (Melrose 1995).

The MCC model makes it possible to distinguish between current flowing between domains (*inter*-flux current) which arises from the relative motions of flux tubes (shuffling) and current flowing within a domain (*intra*-flux current), which arises from internal motion of a single flux tube (i.e. twisting). MCC contains inter-flux currents and no intra-flux currents. This has important implications for the origin of flare energies. A single flux tube can emerge already twisted (Leka *et al.* 1994), but not already shuffled (assuming it is a simple bipole). Thus inter-flux current must be added after emergence through footpoint motions, and the corresponding non-potential energy must be accumulated. It has been claimed that it is impossible for footpoint shuffling to add sufficient energy to account for that observed in large flares (McClymont and Fisher 1989). This assertion can be quantified and tested by applying MCC to a variety of observed flaring active regions. If inter-flux energy were insufficient then the theoretical flare energies $\Delta\mathcal{E}$ would be systematically low, perhaps by orders of magnitude. This would provide compelling evidence that magnetic energy released during a flare had been stored in the field prior to emergence.

Our model is an extension of a current-free model, termed here magnetic charge topology. MCT models contain all of the same geometric features as our model, including separators. The separator is the site of reconnection in MCT, however, its energetics are necessarily absent in a model without current. Observed correlation between separator locations and the signatures of solar flares adds credence to the hypothesis that reconnection is occurring there. It is also noteworthy that the role played by magnetic nulls is somewhat different here than in two dimensional models. Reconnection in MCT models *does not* occur at null points. In fact, had the point charges been placed below the photosphere the null points would be artifacts, while the separator would not.

The possibility of current sheet formation along the separator has been recognized in MCT models (Sweet 1969, Somov 1986, Hénoux and Somov 1987, Gorbachev and Somov 1988). We have presented a quantitative account of how these currents arise, analogous to an electric generator with a perfect short across its terminals (the corona). The magnetic field in the generator is changed mechanically, by the motion of a bar magnet perhaps. This *would* change the flux through the generator coil, and produce an electro-motive force, had the terminals not been shorted. Instead current flows through the coil, and back through the short, to prevent the coil's flux from changing. As a result no voltage drop occurs and a net current $I = -\Delta\Psi^{(v)}/c\mathcal{L}$ is left flowing through the coil. This mechanical component appears to be missing from previous circuit treatments of coronal currents (Alfvén and Carlqvist 1967, Spicer 1982, Melrose 1995).

Observational evidence for separator current ribbons must be sought. Vector magnetographs are capable of measuring horizontal magnetic fields, and thereby determining the vertical current. Such measurements routinely observe 10^{11} amps or more (e.g. Gary *et al.* 1987), however, current densities large enough to be considered sheets are seen rarely if ever. This fact should be balanced with the understanding that magnetographs are better suited to observing intra-flux current than inter-flux current. They are primarily sensitive to the magnetic fields in the photosphere, well below the magnetic canopy. We do not expect inter-flux currents, such as the separator current sheets, to flow below the canopy, since these currents originate in the corona and will seek to close through a path of least resistance. (i.e. the highest level they can without crossing field lines — just beneath the canopy). Certainly a more detailed model is needed to clarify this point and to identify what observable consequences are expected from inter-flux currents.

We use the term current sheet to denote a discontinuity in the equilibrium magnetic field. True discontinuities can occur only in a purely ideal plasma ($\eta = 0$); resistivity would diffuse the sheet to some finite thickness δ. For small enough resistivity, however, the diffusive thickness will be small enough to appear as a discontinuity on large scales. The thickness of a current sheet in laminar steady state is given by the Sweet-Parker theory (Parker 1957, Sweet 1958a)

$$\delta \sim \sqrt{\frac{\eta c^2}{v_{\rm A} w}}\, w = (\rho/\pi)^{1/4} \sqrt{\frac{\eta c^3}{|I|}}\, w \quad , \tag{23}$$

where w is the sheet's width. Using the locally two dimensional expression $w \sim L\sqrt{|I|/I^\star}$ (see Appendix B) gives a parallel electric field

$$E_{\parallel} = \frac{\eta I}{w\delta} \sim \left(\frac{\pi}{\rho}\right)^{1/4} \frac{\sqrt{\eta}}{L^2}\frac{I^\star}{c}\sqrt{\frac{|I|}{c}} \simeq 7\times 10^{-7}\sqrt{\frac{|I|}{10^{10}\,{\rm Amps}}}\ {\rm V/m} \quad , \tag{24}$$

where the final expression uses values from Figures 4 and 5, $L = 10^{10}$ cm and $I^\star = 10^{10}$ Amps, and properties of the active corona, $\rho = 10^{-14}\,{\rm g\,cm^{-3}}$ and $\eta = 3\times 10^{-15}$ sec. For currents $|I| \simeq I^\star = 10^{10}$ Amps the resistive electric field is much less than $\dot{\Psi}^{(\rm v)}/cL \simeq 0.1\,{\rm V/m}$. This means that Sweet-Parker diffusion at the current sheet will not affect the build-up of current during evolution, and the corona will appear to be a perfect conductor ($E_{\parallel} \simeq 0$).

The relaxation assumed to occur during flares must therefore involve a reconnection mode much "faster" than the Sweet-Parker theory (i.e. yielding much larger $E_{\parallel}$). The existence of a fast reconnection mechanism has been a continuing a source of controversy in the study of MHD (Biskamp 1986, Forbes and Priest 1987, Priest and Forbes 1992).

Within the context of the MCC, however, the lack of a fast reconnection would lead to unbounded growth of current and non-potential energy, in contradiction to intuition and observation. Therefore, one interpretation of the stick-slip reconnection model is that Sweet-Parker current sheets are stable only below some threshold current. When this threshold is exceeded, an instability occurs (e.g. Ion-acoustic instability or MHD tearing mode) changing the nature of the reconnection. Our principal justification for this is heuristic: it leads to a model resembling the corona.

The coronal evolution resulting from MCC consists of periods of stressing, punctuated by occasional reconnection events. Indeed, coronal evolution has been cast in these general terms many times (Gold 1964, Rosner and Vaiana 1978, Browning *et al.* 1986, Longcope and Sudan 1992), notably by Parker (1988) in his theory of *nanoflares*. The MCC model is a semi-quantitative implementation of the nanoflare theory in a realistic magnetic geometry. The frequency and energy release of flares are set by a single free parameter θ and the location of current sheets is determined by the topology of the field.

The introduction of stick-slip (or threshold) reconnection permits MCC to follow the long-term evolution of an active region corona. Over long times the magnetic field remains close to a vacuum field. It does this through sporadic relaxation events (nanoflares) which also dissipate stored magnetic energy. For the specific geometry in the shearing scenario the average power dissipation is given by Equation (18). This has the same form as the power lost by a particle in motion resisted by a friction $\theta\bar{F}_{21}$. This analogy is apt since the stick-slip reconnection saps energy from the motion in a manner analogous to classical models of mechanical friction (Marion and Thornton 1988). We expect the dissipated power in a general active region to take a similar form,

$$\bar{P} = -\theta \sum_i \mathbf{v}_i \cdot \bar{F}_i \quad . \tag{25}$$

The friction acting on flux tube i will depend on flux changes induced on all of the separators, $d(\Delta\Psi_\sigma)/d\mathbf{x}_i$, and on their inductive properties, $I^\star_\sigma$ and $\Psi^\star_\sigma$. A coronal heating power linear in the photospheric velocity is common to stress-heating models (Parker 1983) and differs from wave-heating models whose power is quadratic in velocity (Hollweg 1990).

Thus the MCC model can be used to give a numerical estimate for the coronal heating due to the dissipation of "shuffling" energy, yielding an a generalization of Equation (25)

$$\bar{P} \;\sim\; -\theta \int \bar{F}(x,y)\cdot\mathbf{v}(x,y)\,dx\,dy \quad . \tag{26}$$

The friction force density $\bar{F}(x,y) \sim n_{\rm sep}\psi_0^2/L_{\rm sep}^2$ will depend on the statistical distribution of separators through their lengths $L_{\rm sep}$ and the number of separators per unit surface area $n_{\rm sep}$. Accurate determinations of $n_{\rm sep}$ and $L_{\rm sep}$ requires a theoretical ensemble of active regions, synthesized by a random placement of flux tubes. Such a study would predict the heating rate $\bar{P}$ as well as the distributions of flare amplitudes, loop lengths, and frequency of sympathetic flaring. These theoretical predictions could all be readily compared to observations. In the end the threshold θ would be a free parameter which could be used to fit the data. Since the existence of a threshold, and the value of θ, has implications for the details of self-consistent reconnection this procedure promises to shed some light on reconnection as it occurs in the solar corona.

Acknowledgements

The author wishes to thank G.H. Fisher and E.N. Parker for fruitful discussions and to thank G.H. Fisher and the anonymous referee for many helpful comments on the manuscript. This work was supported by a fellowship from the Miller Institute for Basic Research in Science, by Cal Space grant CS-95-17, NASA grant NAGW-3429 and NSF Grant AST-9218085. Part of the work was performed at the Institute for Theoretical Physics under NSF Grant PHY94-07194.

A. Locating Separators

The separator is located numerically by field-line integration from each null. First the nulls are found using a Newton-Raphson method (Press *et al.* 1986) to solve $\mathbf{B}(\mathbf{x}_A) = 0$ and $\mathbf{B}(\mathbf{x}_B) = 0$. The derivative matrices M^A and M^B are evaluated and their eigenvectors calculated. At each null two of the eigenvectors define a plane tangent to the separatrix. For instance, $\hat{\mathbf{e}}_1^A$ and $\hat{\mathbf{e}}_2^A$ define a plane tangent to Σ_A at $\mathbf{x}_A$. Representative field lines are initialized within the tangent plane

$$\mathbf{r}_i^A(0) = \mathbf{x}_A + \delta r[\cos(\varphi_i^A)\hat{\mathbf{e}}_1^A + \sin(\varphi_i^A)\hat{\mathbf{e}}_2^A] \tag{A1}$$

where $\delta r \ll d$ is a small displacement. Each field line is integrated until it intersects the plane bisecting the line $\mathbf{x}_A$–$\mathbf{x}_B$. These points of intersection, $\mathbf{r}_i^A(MP)$ form a piece-wise linear curve $\mathcal{C}^A$, which approximates the intersection of Σ_A with the mid-plane. A similar curve $\mathcal{C}^B$ is formed by field lines $\mathbf{r}_j^B(MP)$ integrated from $\mathbf{x}_B$.

The curves $\mathcal{C}^A$ and $\mathcal{C}^B$ intersect at two points, one above and one below the photosphere. These intersections approximate points on σ_{21} and $\bar{\sigma}_{21}$ respectively. The actual intersection occurs within segments of each curve, say the segment joining $\mathbf{r}_i^A(MP)$ to $\mathbf{r}_{i+1}^A(MP)$ intersects the segment joining $\mathbf{r}_j^B(MP)$ to $\mathbf{r}_{j+1}^B(MP)$. Interpolation to the intersection on each segment defines two new angles $\varphi_{i+1/2}^A$ and $\varphi_{j+1/2}^B$. Using these in Equation (A1) two new field lines $\mathbf{r}_{i+1/2}^A(s)$ and $\mathbf{r}_{j+1/2}^B(s)$ can then be traced to the mid-plane. In general, these field lines will cross the mid-plane at different points, $\mathbf{r}_{i+1/2}^A(MP) \neq \mathbf{r}_{j+1/2}^B(MP)$, however, they will subdivide the intersecting segments of $\mathcal{C}^A$ and $\mathcal{C}^B$. These subdivided segments can then be used to refine the initialization angles (e.g. $\varphi_{i+3/4}^A$ and $\varphi_{j+1/4}^B$) and the process can be repeated. Eventually the field lines will intersect the mid-plane tolerably close, i.e. $|\mathbf{r}^A_{i+\mu}(MP) - \mathbf{r}^B_{j+\nu}(MP)| < \epsilon$, that they can be considered two halves of the same field line: the separator. This algorithm is employed to calculate separators throughout this work.

B. An Approximate Flux-Current Relationship

A quantitative MCC model requires a relationship between the flux $\Psi^{(\mathrm{cr})}_\sigma$ and the current I_σ carried by a ribbon along the separator σ. If the current were carried along a rigid conductor with fixed self-inductance $\mathcal{L}$ the relationship would be $\Psi^{(\mathrm{cr})}_\sigma = c\mathcal{L}\, I_\sigma$. However, the current will change the field around itself, thereby changing its own inductance. Longcope and Cowley (1996) have devised a method of accounting for this effect to exactly calculate the flux-current relationship for a given separator. This calculation is too cumbersome for present purposes; instead we seek an approximate analytic relationship which can be used for all separators. Indeed, Longcope and Cowley have shown such an approximation to be a very good one for the particular geometry they considered.

Our first approximation will be to consider the global structure of the magnetic field, and of the separator loop in particular, to be unaffected by the current itself. The self-flux can then be worked out by integration along the vacuum separator loop

$$2\Psi^{(\mathrm{cr})}_\sigma(I_\sigma) = \oint\limits_{\sigma\,\cup\,\bar{\sigma}} \mathbf{A}^{(\mathrm{cr})}\cdot \mathrm{d}\mathbf{l} \;\simeq\; \frac{I_\sigma}{c}\oint\oint \frac{\mathrm{d}\mathbf{l}\cdot\mathrm{d}\mathbf{l}'}{|\mathbf{x}-\mathbf{x}'|} \quad , \tag{B1}$$

where the factor 2 results from counting flux both above and below the photosphere. In writing the final expression we have approximated the current ribbon as an infinitesimal wire, whose vector potential can be written as an integral over the loop. When $|\mathbf{x}-\mathbf{x}'| \gg w$, the width of the ribbon, this approximation is a good one. However, as $|\mathbf{x}-\mathbf{x}'| \to 0$ the integrand diverges, as it should for a wire, but not for a current ribbon with finite width (Longcope and Cowley 1996). To correct this we must appeal to the local geometry of the current ribbon.

Longcope and Cowley worked out an approximate flux-current relationship for a current ribbon on a circular separator loop. This case demonstrates how the above integral is regularized locally. To make direct use of it we add and subtract, from (B1), the flux integral for a circular loop of length $2L$ (i.e. L is the length of just σ)

$$2\Psi^{(\mathrm{cr})}_\sigma(I_\sigma) = \frac{I_\sigma}{c}\left\{\; 2L\,\ln(s) \;+\; 2\int\limits_0^{2L}\mathrm{d}\bar{l}\int\limits_0^{L}\mathrm{d}(\Delta l)\,\frac{1-2\sin^2(\pi\Delta l/2L)}{2L\sin(\pi\Delta l/2L)/\pi}\;\right\} \tag{B2}$$

where $\bar{l} \equiv (l+l')/2$ and $\Delta l \equiv l - l'$. The factor $\ln(s)$ is defined as an integral expressing the difference between the actual separator and a circular loop

$$\ln(s) \equiv \frac{1}{2L}\int_0^{2L} \mathrm{d}l \int_0^{2L} \mathrm{d}l' \left\{ \frac{\hat{\mathbf{n}}\cdot\hat{\mathbf{n}}'}{|\mathbf{x}-\mathbf{x}'|} - \frac{1-2\sin^2(\pi\Delta l/2L)}{2L\,\sin(\pi\Delta l/2L)/\pi} \right\} \quad . \tag{B3}$$

This integral, performed over the path of the separator loop from the vacuum field $\sigma \cup \bar{\sigma}$, is convergent. For the case in which the separator loop really is a circle, $s = 1$, while for the shearing scenario we find values of s ranging from 0.7 to 1, depending on Δx.

The integral term in Equation (B2) diverges at the limit $\Delta l \to 0$. Our second approximation will be to regularize this integral by defining a lower cutoff $\Delta l_0(\bar{l})$. This cutoff is related to the local width of the current ribbon. We will further assume $\Delta l_0 \ll L$ allowing the $\mathrm{d}(\Delta l)$ integration in Equation (B2) to be performed

$$\Psi_\sigma^{(\mathrm{cr})} = \frac{I_\sigma}{2c}\left\{ 2L\ln(s) + \int_0^{2L} \ln[\,16L^2\,e^{-4}/\pi^2\Delta l_0^2(\bar{l})\,]\,\mathrm{d}\bar{l} \right\} \quad . \tag{B4}$$

When the separator loop is a circle the remaining integral term should yield the result obtained by Longcope and Cowley. The results of their more rigorous treatment can be recovered by making Δl_0 proportional to the width of the current ribbon. Furthermore, Longcope and Cowley found that the current ribbon width was approximately the same as the width of the two dimensional magnetic island formed by a wire carrying the same current.

To calculate the island width, consider a plane perpendicular to the separator, with coordinates (ξ, η) and a magnetic field $\mathbf{B}_\perp(\xi, \eta)$ vanishing at the origin (separator). If the vacuum part of $\mathbf{B}_\perp$ is hyperbolic,

$$\mathbf{B}_\perp = (B_\xi, B_\eta) \simeq (\,B'_\perp\xi,\ -B'_\perp\eta\,) \quad ,$$

where we have chosen to orient the coordinate axis along the characteristic directions. We have also assumed $\mathbf{B}_\perp$ to be divergence-free in the perpendicular plane, as if it really were two dimensional. A current parallel to the separator will contribute a perpendicular magnetic field

$$\mathbf{B}_\perp = \frac{I}{2\pi c(\xi^2+\eta^2)}(-\eta, \xi) \quad .$$

Summing these contributions gives a two dimensional magnetic island surrounding the current, whose width (i.e. distance between hyperbolic points) is

$$w = \sqrt{\frac{2|I|}{\pi c B'_\perp}} \quad .$$

Longcope and Cowley go on to refine the single island approximation by using multiple wires which form a chain of islands, and then increasing the number of wires to form a continuous current sheet. However, for sufficiently small currents, they find the results from a single wire to be a good approximation to a genuine current ribbon. At any point on the separator, the coefficient $B_\perp'$ can be determined from the vacuum magnetic field gradient at the separator

$$B_\perp'(\bar{l}) \equiv \sqrt{-\det\{\nabla_\perp \mathbf{B}_\perp^{(\mathrm{v})}\}} \quad , \tag{B5}$$

where $\nabla_\perp \mathbf{B}_\perp^{(\mathrm{v})}$ is the matrix of derivatives within the plane perpendicular to the separator.

We will take the cutoff in Equation (B4) to be proportional to the island width w. Since the cutoff appears inside the logarithm the exact constant of proportionality is not critical. To match the results of Longcope and Cowley (1996) we choose

$$\Delta l_0^{-2} = \frac{2eB_\perp'(\bar{l})c}{|I_\sigma|} \;=\; \frac{4}{\pi}\,w^{-2} \quad . \tag{B6}$$

Replacing this in Equation (B4) leads to

$$\Psi_\sigma^{(\mathrm{cr})} = \frac{I_\sigma}{2c}\int_0^{2L} \ln[\,32e^{-3}\,(L/\pi)^2 sB_\perp'(\bar{l})c/|I_\sigma|\,]\,\mathrm{d}\bar{l} = \frac{L\,I_\sigma}{c}\ln[\,32e^{-3}\,(L/\pi)^2 s\bar{B}_\perp' c/|I_\sigma|\,] \quad , \tag{B7}$$

where $\bar{B}_\perp'$ is a geometric mean of the magnetic gradient at the separator

$$\ln[\bar{B}_\perp'] \;\equiv\; \frac{1}{L}\int_0^L \ln[B_\perp'(\bar{l})]\,\mathrm{d}\bar{l} \quad . \tag{B8}$$

The inductive properties of the current ribbon can thus be summarized by calculating the three quantities L, s and $\bar{B}_\perp'$ from the separator of the vacuum field. These quantities can be used to define a characteristic current $I_\sigma^\star$ and flux $\Psi_\sigma^\star$ for the separator

$$I_\sigma^\star \equiv \frac{c\bar{B}_\perp' L^2 s}{8\pi^2} \quad , \quad \Psi_\sigma^\star \equiv \frac{LI_\sigma^\star}{c} \quad , \tag{B9}$$

where, once again, constants have been chosen to correspond to those in Longcope and Cowley (1996). Using these quantities the flux-current relation may be expressed in the simple algebraic form

$$\Psi_\sigma^{(\mathrm{cr})}(I_\sigma) = \Psi_\sigma^\star \frac{I_\sigma}{I_\sigma^\star}\ln\left[\,256e^{-3}\,\frac{I_\sigma^\star}{|I_\sigma|}\right] \;\equiv\; \Psi_\sigma^\star\,\Lambda(I_\sigma/I_\sigma^\star) \quad , \tag{B10}$$

where the function $\Lambda(x)$ will be the same for every separator. Application of this relationship will involve inverting the function $\Lambda(x)$, which is not one-to-one. However, we can safely restrict the argument to the range $|x| < 4.69$ over which $\Lambda(x)$ is monotonic. Thus we will assume Equation (B10) to apply only to this domain.

This is the current-flux relation for a current ribbon which follows the original separator. The width of the current ribbon varies along the separator according to

$$w(l) = \frac{L}{2}\sqrt{\frac{s}{e\pi^3}}\left[\frac{B'_\perp(l)}{\bar{B}'_\perp}\right]^{-1/2}\left(\frac{|I_\sigma|}{I^\star_\sigma}\right)^{1/2} \quad . \tag{B11}$$

The coefficient $[B'_\perp(l)/\bar{B}'_\perp]^{-1/2}$ contains the variation in ribbon width; it has a geometric average of unity according to Equation (B8). As long as $|I_\sigma| \ll I^\star_\sigma$ the ribbon will be narrow in the sense that $w \ll L$. The ribbon will be widest where $B'_\perp(l)$ is the smallest. For a potential field extrapolated from $z = 0$ this derivative will generally be smaller at higher altitudes, so the ribbon should broaden with height.

The analysis above has assumed that the magnetic field, $\mathbf{B}_\perp$, in a plane normal to the separator, is locally hyperbolic. This is necessary in order to determine the width of the current ribbon as a function of the current alone. By the definition of the separator field line $\mathbf{B}_\perp$ is hyperbolic near the null points. In some instances, however, this property can fail to hold at points away from the nulls. In this case the width w of a current sheet will depend on factors other than the current, even in the limit $|I| \to 0$. Such instances are troublesome for the present analysis: $B'_\perp(\bar{l})$ can no longer be defined according to Equation (B5) since $\det\{\nabla_\perp \mathbf{B}^{(v)}_\perp\} > 0$. This failure is symptomatic of a ribbon whose properties are not continuous functions of current; a case we call *structurally unstable*. It should be noted that structural instability of a separator is a function only of its vacuum configuration. Thus in the shearing scenario it occurs for a certain range of Δx, independent of the current I_{21} (i.e. the choice of Δx_0).

Structural instability is a genuinely three-dimensional effect. In two dimensions the neighborhood of a current sheet is required to be hyperbolic in order that $\mathbf{B}_\perp$ be divergence-free. The same cannot be said of three-dimensions, where $\partial B_{||}/\partial l$ also plays a role in the divergence. Since the theory of Longcope and Cowley works by analogy to two dimensions it does not seem capable of predicting the structure of a current ribbon along a structurally unstable separator. The fact remains, however, that to prevent a change in flux some current *must* flow. At present we are simply unable to exhibit even an approximate current-flux relationship, therefore we will adopt the expedient measure of setting $I^\star_\sigma$ to some small value in cases of structurally unstable separators.

REFERENCES

Alfvén, H. A. and Carlqvist, P.: 1967, *Solar Phys.* **1**, 220.

Altschuler, M. D. and Newkirk, G.: 1969, *Solar Phys.* **9**, 131.

Antiochos, S. K.: 1987, *Astrophys. J.* **312**, 886.

Bagalá, L. G., Mandrini, C. H., Rovira, M. G., Démoulin, P., and Hénoux, C. H.: 1995, *Solar Phys.* **161**, 103.

Baum, P. J. and Bratenahl, A.: 1980, *Solar Phys.* **67**, 245.

Biskamp, D.: 1986, *Phys. Fluids* **29**(5), 1520.

Brown, J. C., Correia, E., Fŕnik, F., Garcia, H., Hénoux, J.-C., La Rosa, T. N., Machado, M. E., Nakima, H., and Priest, E. R.: 1994, *Solar Phys.* **153**, 19.

Browning, P. K., Sakurai, T., and Priest, E. R.: 1986, *Astron. Astrophys.* **158**, 217.

Caligari, P., Moreno-Insertis, F., and Schüssler, M.: 1995, *Astrophys. J.* **441**, 886.

Cowley, S. W. H.: 1973, *Radio Sci.* **8**(11), 903.

Démoulin, P., Hénoux, J., and Mandrini, C.: 1994a, *Astron. Astrophys.* **285**, 1023.

Démoulin, P., Mandrini, C. H., Rovira, M. G., Hénoux, J. C., and Machado, M. E.: 1994b, *Solar Phys.* **150**, 221.

Démoulin, P., van Driel-Gesztelyi, L., Schmieder, B., Hénoux, J. C., Csepura, G., and Hagyard, M. J.: 1993, *Astron. Astrophys.* **271**, 292.

D'Silva, S. and Choudhuri, A. R.: 1993, *Astron. Astrophys.* **272**, 621.

Fan, Y., Fisher, G. H., and McClymont, A. N.: 1994, *Astrophys. J.* **436**, 907.

Forbes, T. G. and Priest, E. R.: 1987, *Rev. Geophys.* **25**(8), 1583.

Gabriel, A. H.: 1976, *Phil. Trans. R. Soc. Lond.* **A281**, 339.

Gary, G. A., Moore, R. L., Hagyard, M. J., and Haisch, B. M.: 1987, *Astrophys. J.* **314**, 728.

Giovanelli, R. G.: 1980, *Solar Phys.* **68**, 49.

Giovanelli, R. G. and Jones, H. P.: 1982, *Solar Phys.* **79**, 267.

Gold, T.: 1964, in Hess, W. N. (ed.), *AAS-NASA Symposium on the Physics of Solar Flares*, pp. 389–395. NASA.

Gold, T. and Hoyle, F.: 1960, *Momthly Notices Roy. Astron. Soc.* **120**(2), 89.

Gorbachev, V. S. and Somov, B. V.: 1988, *Solar Phys.* **117**, 77.

Hanaoka, Y.: 1994, *Astrophys. J.* **420**, L37.

Hénoux, J. C. and Somov, B. V.: 1987, *Astron. Astrophys.* **185**, 306.

Hollweg, J. V.: 1990, *Comp. Phys. Rep.* **12**, 205.

Hood, A. W. and Priest, E. R.: 1979, *Solar Phys.* **64**, 303.

Jackson, J. D.: 1975, *Classical Electrodynamics*, Wiley, New York.

Kopp, R. A. and Kuperus, M.: 1968, *Solar Phys.* **4**, 212.

Lau, Y.-T.: 1993, *Solar Phys.* **148**, 301.

Leka, K. D., Van Driel Gesztelyi, L., and Canfield, R. C.: 1994, in Balasubramaniam, K. S. and Simon, G. W. (eds), *Solar Active Region Evolution: Comparing Models with Observations*, pp. 145–148.

Longcope, D. W. and Cowley, S. C.: 1996, *Phys. Plasmas* **3**(8), 2885.

Longcope, D. W. and Strauss, H. R.: 1994, *Astrophys. J.* **437**, 851.

Longcope, D. W. and Sudan, R. N.: 1992, *Phys. Fluids B* **4**(7), 2277.

Low, B. C.: 1977, *Astrophys. J.* **212**, 234.

Machado, M. E., Somov, B. V., Rovira, M. G., and De Jager, C.: 1983, *Solar Phys.* **85**, 157.

Mandrini, C. H., Démoulin, P., Hénoux, J. C., and Machado, M. E.: 1991, *Astron. Astrophys.* **250**, 541.

Marion, J. B. and Thornton, S. T.: 1988, *Classical Dynamics of Particles and Systems*, Harcourt Brace Jovanovich, San Diego, third edition.

McClymont, A. N. and Fisher, G. H.: 1989, in Waite, J. H., Burch, J. L., and Moore, R. L. (eds), *Solar System Plasma Physics*, p. 219, Washington. AGU.

Melrose, D. B.: 1992, *Astrophys. J.* **387**(403–413).

Melrose, D. B.: 1995, *Astrophys. J.* **451**, 391.

Mikic, Z. and McClymont, A. N.: 1994, in Balasubramaniam, K. S. and Simon, G. W. (eds), *Solar Active Region Evolution: Comparing Models with Observations*, pp. 225–232.

Nakagawa, Y. and Raadu, M. A.: 1972, *Solar Phys.* **25**, 127.

Parker, E. N.: 1955, *Astrophys. J.* **121**, 491.

Parker, E. N.: 1957, *J. Geophys. Res.* **62**(4), 509.

Parker, E. N.: 1983, *Astrophys. J.* **264**, 635.

Parnell, C. E., Priest, E. R., and Golub, L.: 1994, *Solar Phys.* **151**, 57.

Press, W. H., Flannery, B. P., Teukolsky, S. A., and Vetterling, W. T.: 1986, *Numerical Recipes: The art of scientific computing*, Cambridge University Press, Cambridge.

Priest, E. R. and Forbes, T. G.: 1989, *Solar Phys.* **119**, 211.

Priest, E. R. and Forbes, T. G.: 1992, *J. Geophys. Res.* **97**(A11), 16757.

Rosner, R. and Vaiana, G. S.: 1978, *Astrophys. J.* **222**, 1104.

Schmidt, H. U.: 1964, in Hess, W. N. (ed.), *AAS-NASA Symposium on the Physics of Solar Flares*, p. 107. NASA.

Shimizu, T., Tsuneta, S., Acton, L. W., Lemen, J. R., Ogawara, Y., and Uchida, Y.: 1994, *Astrophys. J.* **422**, 906.

Shimizu, T., Tsuneta, S., Acton, L. W., Lemen, J. R., and Uchida, Y.: 1992, *Proc. Astron. Soc. Japan* **44**, L147.

Somov, B. V.: 1986, *Astron. Astrophys.* **163**, 210.

Somov, B. V.: 1992, *Physical Processes in Solar Flares*, Kluwer.

Spicer, D. S.: 1982, *Space Sci. Rev.* **31**, 351.

Sweet, P. A.: 1958a, in Lehnert, B. (ed.), *Electromagnetic Phenomena in Cosmical Physics*, pp. 123–134. Cambridge University Press, Cambridge, U.K.

Sweet, P. A.: 1958b, *Nuovo Cimento* **8**, 188.

Sweet, P. A.: 1969, *Ann. Rev. Astron. Astrophys.* **7**, 149.

Syrovatskii, S. I.: 1971, *Sov. Phys. JETP* **33**(5), 933.

Van Ballegooijen, A. A.: 1985, *Astrophys. J.* **298**, 421.

Van Hoven, G. *et al.*: 1980, in Sturrock, P. A. (ed.), *Solar Flares. A monograph from Skylab Solar Workshop II*, pp. 17–81. Colorado Associated University Press.

Yeh, T.: 1976, *J. Geophys. Res.* **81**(13), 2140.

This preprint was prepared with the AAS LaTeX macros v4.0.

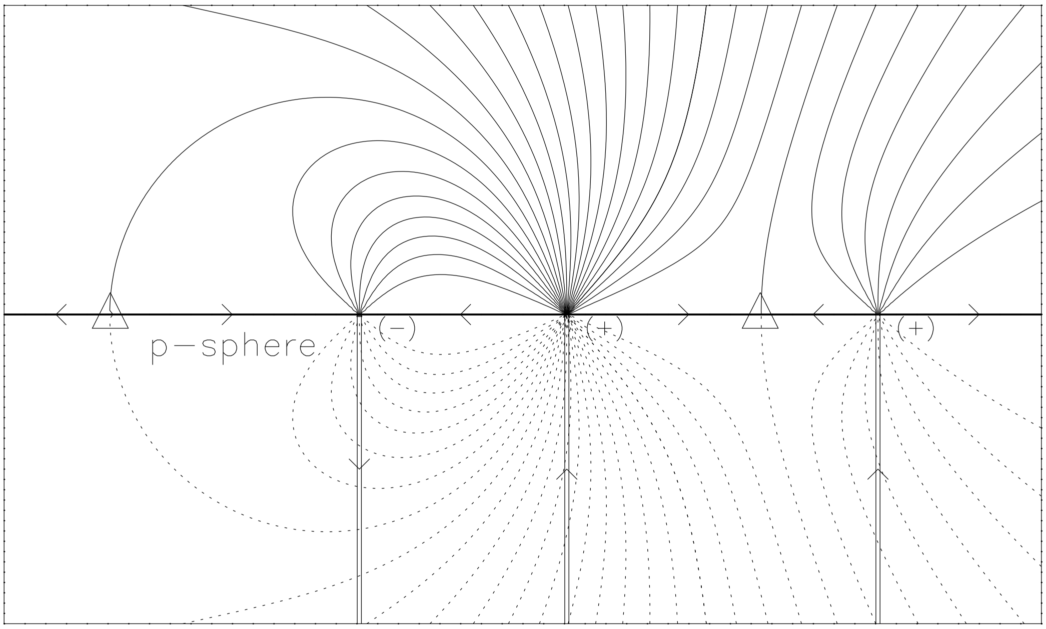

Fig. 1.— An example of the coronal field model formed by three co-linear point charges. Field lines are shown with solid lines above the photosphere ($z > 0$). Below the photosphere ($z < 0$) the field vanishes except inside the three vertical flux tubes, shown by solid double lines. In the two tubes on the right field is directed upwards so the corresponding point charges are positive. The two magnetic null points ($\triangle$) lie on the photosphere. The mirror coronal field is shown with dotted lines beneath the photosphere (cf. Figure 1. of Sweet 1958, Figure 5. of Gabriel 1976 and Figure 4. of Parker 1978)

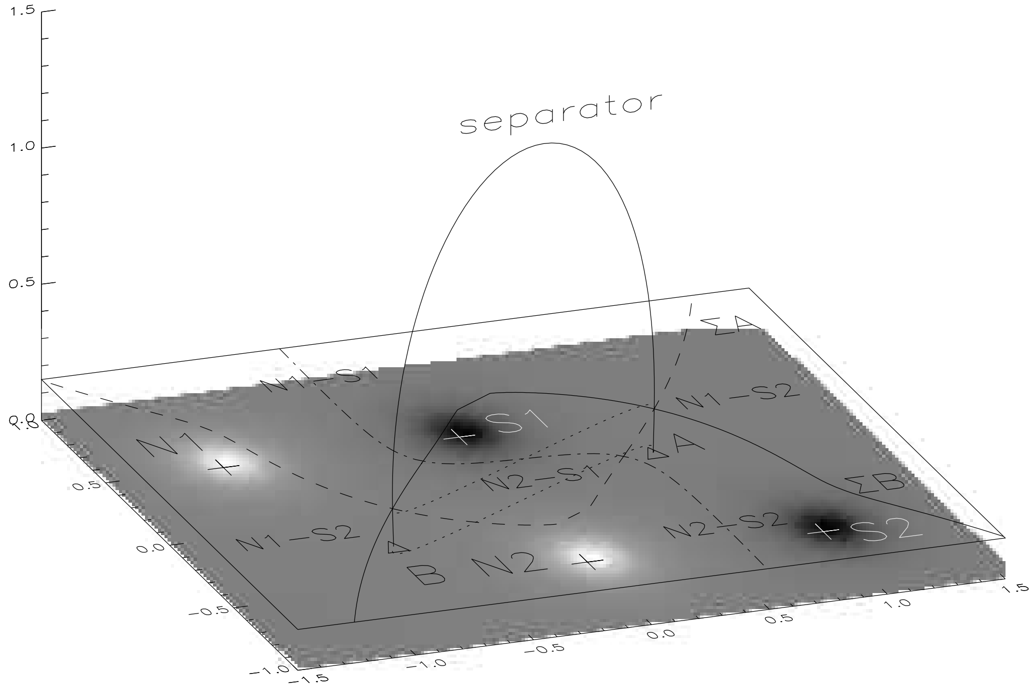

Fig. 2.— The magnetic topology of two parallel bipoles. The locations of the charges, $N1$, $N2$, $S1$ and $S2$ are marked by $+$'s. The grey-scale is a synthesized magnetogram representing B_z at the visualization plane $z = z_v = 0.15$, but projected onto $z = 0$ for clarity. The two magnetic nulls, A and B, are marked with $\triangle$'s. Their separatrix surfaces, Σ_A and Σ_B, intersect the visualization plane along the dashed and solid curves respectively. These partition the plane into domains labeled $N1 - S1$ etc. according to the terminal points of their field lines. The magnetic neutral line, shown as a broken curve with a lazy-S shape, denotes the place where $B_z = 0$ on the visualization plane. Field lines cross over the magnetic neutral line from left to right (North to South). The separator field line (solid) is the intersection of Σ_A and Σ_B.

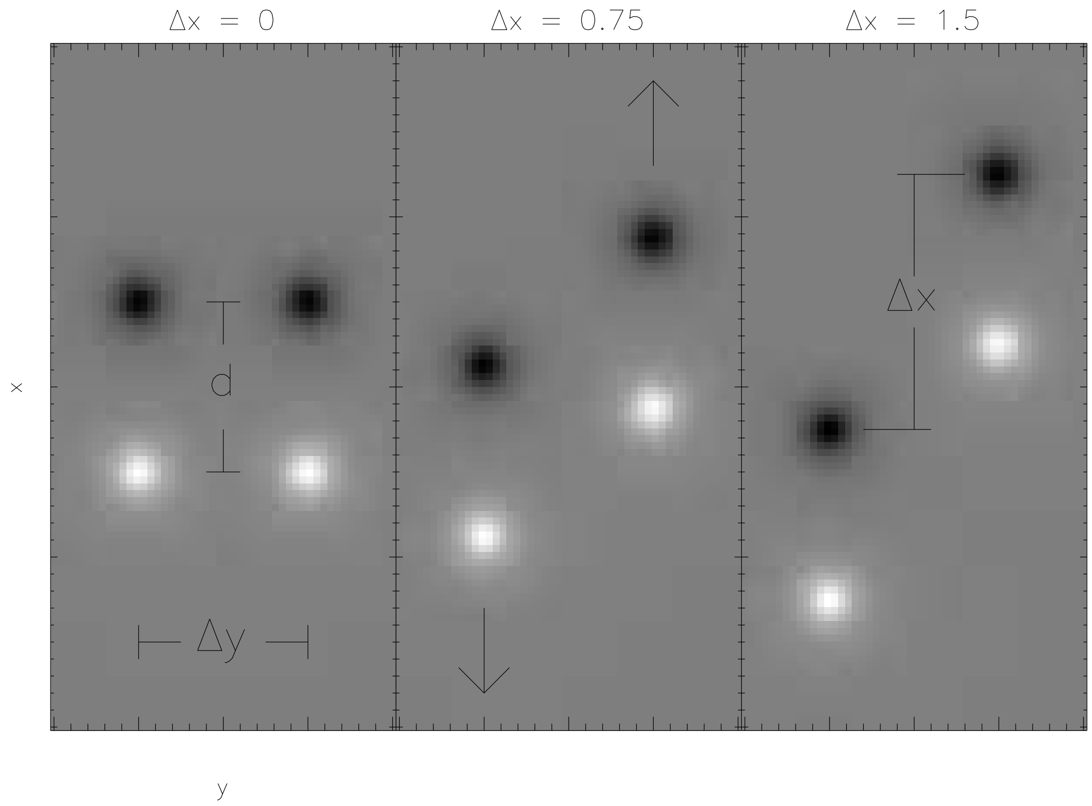

Fig. 3.— The motion of the two parallel bipoles past one another. Synthetic magnetograms are shown for configurations $\Delta x = 0$, $\Delta x = 0.75\,d$ and $\Delta x = 1.5\,d$. These are rotated 90° so the y axis is horizontal.

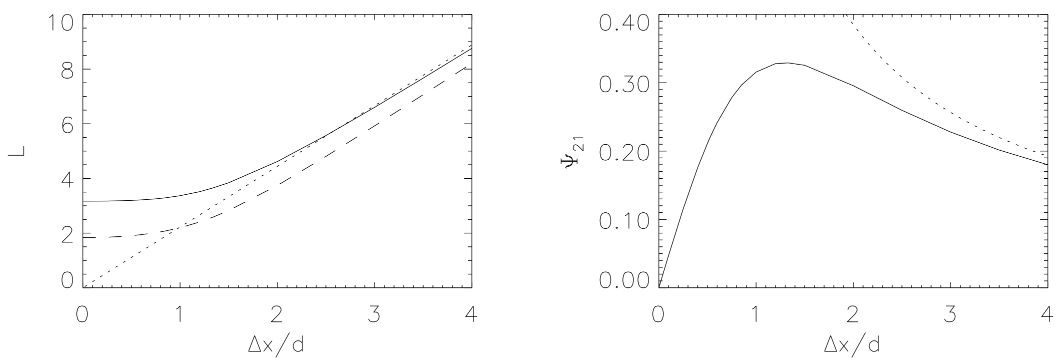

Fig. 4.— Properties of the separator σ_{21} for the shearing scenario as a function of relative displacement Δx. (a) The length of the separator loop L in units of d (solid). For comparison a dashed line shows the length of a semi-circle connecting the nulls, $2\pi|\mathbf{x}_A|$. (b) The flux through the separator loop, Ψ_{21} in units of ψ_0. The axisymmetric problem of two co-axial dipoles provides a limiting case; this is plotted with dotted lines.

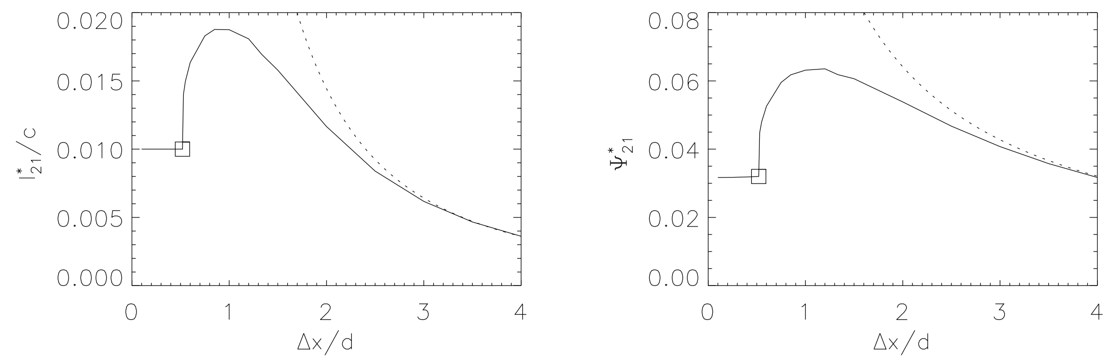

Fig. 5.— The inductive properties of the separator loop (a) $I^{\star}_{21}$ (in units of ψ_0/d) and (b) $\Psi^{\star}_{21}$ as functions of the relative shear, Δx. Left of $\Delta x = 0.53\,d$ (marked by a box) the separator is structurally unstable so $I^{\star}_{21}$ is set to 0.01 by default (see Appendix B).

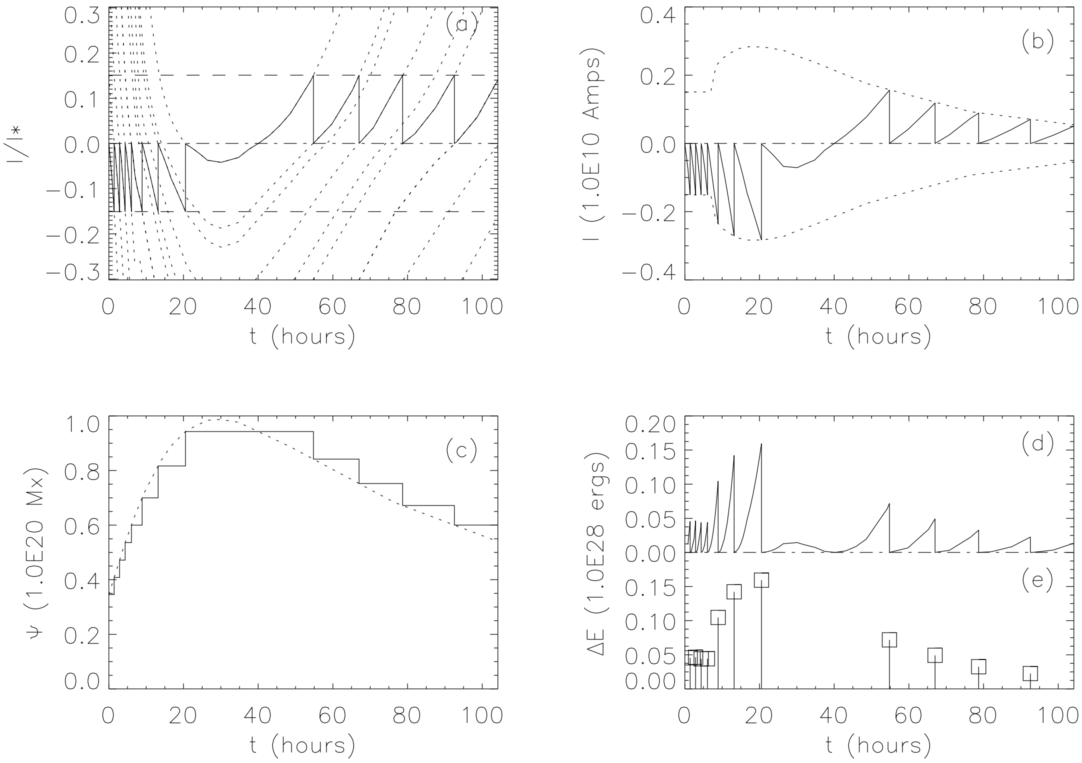

Fig. 6.— The time evolution of two small bipoles. (a) The dimensionless current $I_{21}/I^{\star}_{21}$ (solid). Flares occur when this crosses $\pm\theta$ (dashed lines). Dotted curves show the continuation of the curve past the threshold (broken line). Each dotted curve represents a unique value of Ψ^{0}_{21}; once reconnection changes this value the path leaves that curve for good. (b) The dimensional current I_{21} (solid) and the threshold currents $\pm\theta I^{\star}_{21}$ (dotted). (c) The flux Ψ_{21} enclosed by σ_{21} (solid) and the value for a vacuum field $\Psi^{(\mathrm{v})}_{21}$ (dotted). (d) The non-potential energy of the field, $\Delta\mathcal{E}$; its downward transitions are flares. (e) The energies of each flare.

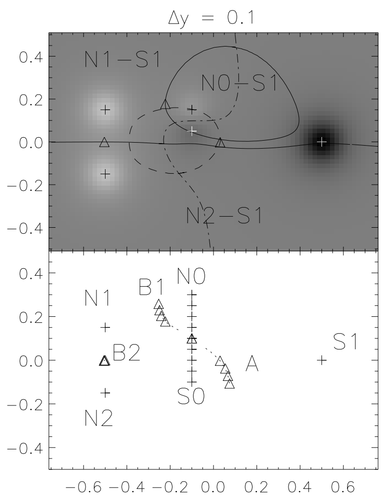

Fig. 7.— The magnetic configuration for the emergence scenario. (a) A synthetic magnetogram from $\Delta y = 0.1\,d$. Locations of the poles and nulls at this time are shown by $+$'s and $\triangle$'s respectively. The magnetic neutral line is shown by a broken line, and the separatrices are shown by solid (Σ_{B1} and Σ_{B12}) and dashed (Σ_A) lines. These partition the flux into 6 domains, but only the domains associated with $S1$ are labeled. (b) the locations of the poles and nulls for $\Delta y = 0$, 0.1, 0.2, 0.3, 0.4. The poles $N0$ and $S0$ change locations, as do all the null points, although $B2$ does so only slightly. At $\Delta y = 0$ the four points $N0$, $S0$, A and $B1$ coincide at the point of emergence: $(-0.1, 0.1)$.

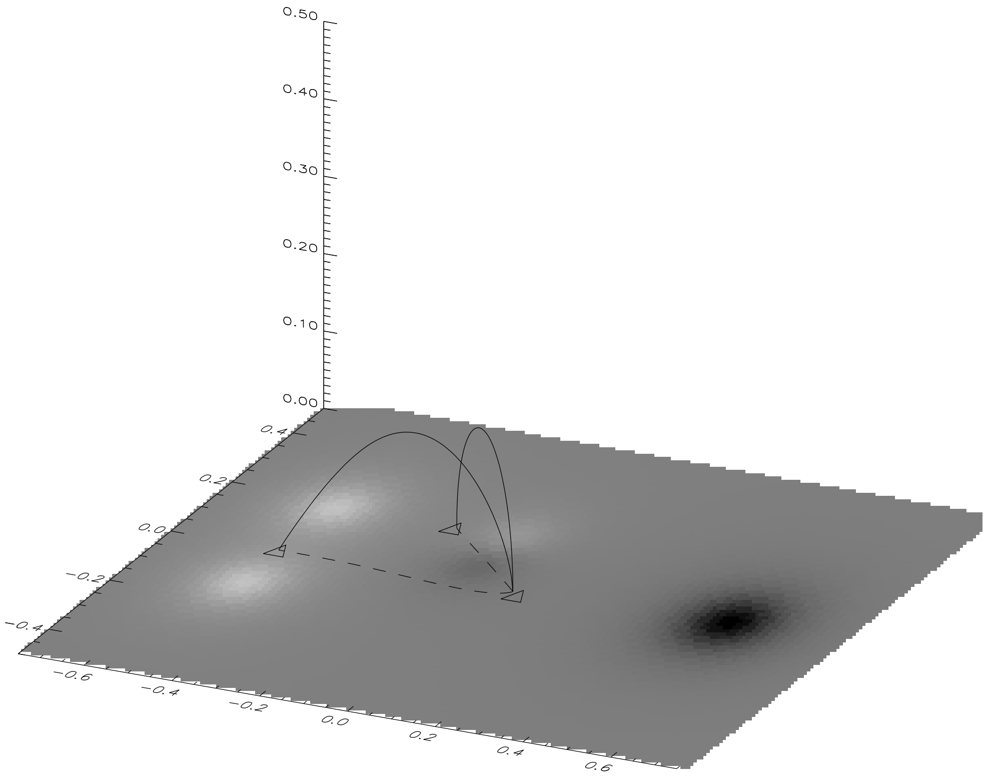

Fig. 8.— A view of the separator field lines σ_{00} and σ_{20} at $\Delta y = 0.1$ in the emergence scenario. The synthesized magnetogram from Figure 7a is projected onto the photosphere $z = 0$. The locations of the nulls are shown by $\triangle$'s.

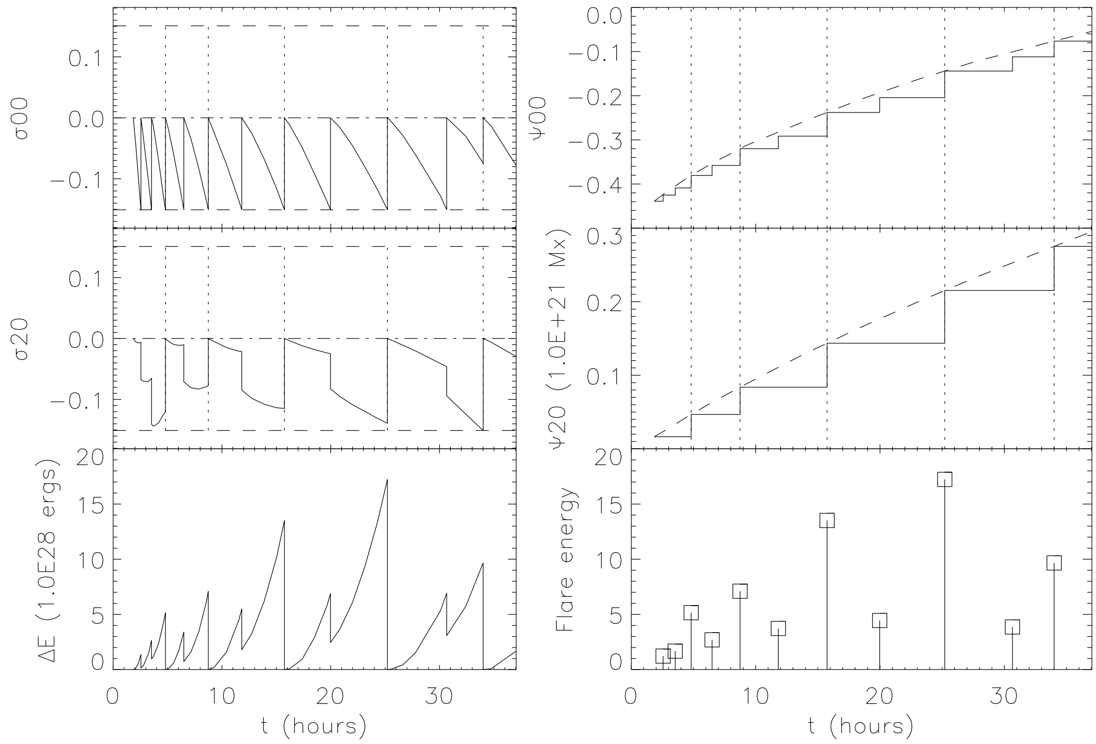

Fig. 9.— The time evolution of the emergence scenario. The dimensionless current, (a) $I_{00}/I^{\star}_{00}$ and (c) $I_{20}/I^{\star}_{20}$ along with the threshold $\theta = 0.15$. Each current changes discontinuously during a flare, but only during a sympathetic flare, shown with dotted vertical lines, are both currents are set to zero. The fluxes (b) Ψ_{00} and (d) Ψ_{20} (solid) are constant except for discontinuous changes during a flare on that separator. During a sympathetic flare it achieves its vacuum value $\Psi^{(v)}$ (dashed). The total non-potential energy of the system (e) decreases abruptly during each flare. The drop in non-potential energy is the flare energy, shown as a spike in (f).